Title

Amphiphilic Protein Microfibrils from Ice-Templated Self-Assembly and Disassembly of Pickering Emulsions

Journal

ACS Applied Bio Materials, 3(4)

ISSN

2576-6422

Authors

Liu, Xingchen
Hsieh, You-Lo

Publication Date

2020-04-20

DOI

10.1021/acsabm.0c00188

Peer reviewed

ACS APPLIED BIO MATERIALS

www.acsabm.org Article

Amphiphilic Protein Microfibrils from Ice-Templated Self-Assembly and Disassembly of Pickering Emulsions

Xingchen Liu and You-Lo Hsieh*

Cite This: *ACS Appl. Bio Mater.* 2020, 3, 2473−2481 Read Online

ACCESS | Metrics & More | Article Recommendations | Supporting Information

ABSTRACT: Amphiphilic protein microfibrils have been generated for the first time by ice-templated self-assembly of aqueous globular protein colloids and subsequent selective disassembly in polar solvents like MeOH, EtOH, acetone, and dimethylformamide. Semicrystalline microfibrils, ca. 1.2 μm wide and 45−70 μm long, produced from soy proteins are excellent amphiphiles, which are capable of stabilizing both high-internal-phase o/w and $w_1/o/w_2$ double emulsions as well as retaining amphiphilicity even with surface-bound lipophiles and electrophiles. This ice-templated self-assembling and polar solvent disassembling approach is applicable to other legume proteins, such as pea proteins, and is scalable to process globular proteins into amphiphilic microfibrils for Pickering emulsions in many potential applications including food, pharmaceuticals and skin care.

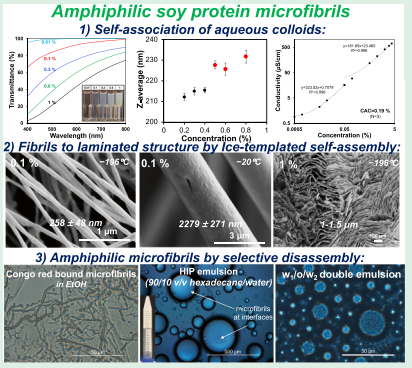

KEYWORDS: *soy proteins, amphiphilicity, ice-templated self-assembly, disassembly, Pickering emulsion*

1. INTRODUCTION

Globular proteins such as soy proteins (SPs) are too large and complex in molecular structure to be processed into materials as in the case of fibrillar proteins. SPs constitute 46−54% of soybean meals, the major byproducts of the largest edible oil and biodiesel production in the United States,[1] thus are the most abundantly available plant proteins, but least utilized with only less than 2% destined for domestic human food consumption.[2] SPs consist of several proteins, of which two major proteins, that is, ca. 52% glycinin (350 k*Da*) and 35% β-conglycinin (180−210 k*Da*),[3] have much higher molecular weight than common globular proteins, such as casein (19−25 k*Da*) and zein (19−27 k*Da*).[4] Their large size and conformational heterogeneity make SPs particularly challenging to process in general and to fabricate into fibrous materials specifically.

We have successfully demonstrated that the SP isolate (SPI) can be robustly processed into highly stable aqueous (aq.) colloids at up to 9% by high-speed blending (30k rpm, 15 min).[5] Aq. SP colloids are amphiphilic, capable of reducing water surface tension up to 41.2 mN/m at above 0.98% and being solvent-exchanged to less polar 4:1 v/v methanol/water or dimethylformamde (DMF) at 1 w/v %.[5] Amphiphilicity is recognized as one of the most critical molecular bases for self-assembly[6] of amphiphiles, such as phosphatidylcholine into lipid bilayers in biological systems.[7] Globular proteins, such as β-lactoglobulin, bovine serum albumin, lysozyme, and ovalbumin, are known to self-assemble at their native and/or partially denatured states.[8] Native SPs have shown to aggregate into 2−5 fold larger in mass and hydrodynamic radius with either increasing concentrations (1−100 g/L) or decreasing charges in the 5.8−7.0 pH range.[9] An equal mixture of partially denatured and hydrolyzed (pH = 2, 80 °C, 12 h) soy β-conglycinin and glycinin was shown to form 1.6−1.8 nm thick and 100−800 nm long amyloid-like fibrils.[10] However, if and how these behaviors may lead to materials has never been studied.

Here, self-assembling of amphiphilic aq. SP colloids is further exploited for structural engineering into materials. The amphiphilic behaviors of aq. SP colloids over a full concentration gradient were first detailed by visible light transmittance, dynamic light scattering, and electrical conductivity; then how ice-templating led to self-assembled structures was investigated. Ice templating has shown to induce self-assembling of amphiphilic cellulose nanofibrils[11] and replacing water with tert-butanol reduced self-assembled fiber sizes and also enabled dispersing in DMF.[12] The ice-templating induced self-assembled structures of aq. SP colloids over a wide range of concentrations were thoroughly analyzed by scanning electron and optical microscopy and their pore structure and specific surface by N_2 adsorption−desorption isotherms, crystallinity, secondary structure composition, and

Received: February 18, 2020
Accepted: March 11, 2020
Published: March 11, 2020

https://dx.doi.org/10.1021/acsabm.0c00188
ACS Appl. Bio Mater. 2020, 3, 2473−2481

thermal behavior. The nature of interfaces in the ice-templated assemblies was elucidated by their ability to be dispersed in solvents with different dielectric constants and H-bonding abilities. The amphiphilic characteristics of disassembled solids were evaluated by their ability to bind lipophilic and hydrophilic dye molecules and to serve as either hydrophilic or lipophilic Pickering emulsifiers to stabilize high-internal-phase (HIP) and double emulsions. Furthermore, feasibility of this approach to other globular proteins was tested using legume yellow pea proteins.

2. MATERIALS AND METHODS

2.1. Materials. SPI (MP Biomedicals, LLC) and pea protein isolate (PPI, Naked Nutrition) contained 92 and 90% proteins, respectively. Methanol (MeOH, HPLC grade), ethanol (EtOH, anhydrous, histological grade), acetone (certified), toluene (certified), hexane (certified), hexadecane (certified), and methylene blue (MB, certified biological stain) were purchased from Fisher Scientific. DMF (HPLC grade, EMD), chloroform (HPLC grade, EMD), Sudan Red 7B (SR, Aldrich Chemical Corporation, Inc.), and Congo red (CR, Eastman Chemical Company) were used as received without further purification. Regenerated cellulose membranes (Fisherbrand) with a 3.5 kDa cut-off were used for dialysis. All water used was purified by the Millipore Milli-Q plus water purification system.

2.2. Aq. SP Colloids and Freeze-Dried Products. Crude SPI or PPI was stirred into water at ca. 10%, dialyzed at 8−11 °C for 24 h, then either magnetically stirred (∼2k rpm, 1 h) as control dispersions or further processed by either blending (30k rpm, 15 min) using a high-speed blender (Vitamix 5200) or pulse sonication (on 1 min, off 15 s) for 5 min at 60 or 120 W or 50 or 100% amplitude using a probe sonicator (Q700, Sonicator Co., Ltd.). The blended and sonicated dispersions were centrifuged (5k rpm, 15 min) to collect the supernatants as aq. SP colloids. All lower-concentration control and aq. SP colloids were diluted from those prepared at 5%. The exact SP or PP concentrations were determined from the dried mass (65 °C) of 1 g of aq. dispersion or colloid in triplicates to calculate the average w/w % or simply %, unless stated otherwise. SR, CR, or MB was, respectively, added to 1% (ca. 0.04 mM) SP colloids at 0.8 mM and then bath-sonicated (40 kHz, 130 W max, Branson ultrasonic processor model 2510) for 15 min.

Aq. control dispersions and colloids (25 mL, 0.001−9%) and aq. SP/dye colloids were placed in polypropylene centrifuge tubes (3 cm diameter) and frozen in liquid nitrogen (−196 °C) for 5 min, then lyophilized at −50 °C (Free Zone 1.0 L Benchtop Freeze Dry System, Labconco) for 2 days into the so-called freeze-dried or ice-templated products. To speed up freezing to 1 min, aluminum tubes (4.5 cm diameter) were used.

2.3. Dispersion and Pickering Emulsion Preparation. The dispersibility of ice-templated products (0.1 or 1 w/v %) in aq. and organic solvents (DMF, MeOH, EtOH, acetone, chloroform, toluene, and hexane) was evaluated following 5 or 15 min of bath sonication. To evaluate their compatibility with selected solvents, ice-templated SPs dispersions in EtOH at 1 w/v % were centrifuged (5k rpm, 15 min) to collect precipitates to be re-dispersed in water, chloroform, toluene, hexane, and EtOH/hexane (2:1, v/v) by vortexing (∼3.2k rpm, 1 min). These centrifugation and re-dispersion were repeated twice. The dye binding efficiency of SP colloids was determined by quantifying the amount of unbound dyes that remain in supernatants (5k rpm, 15 min) using Evolution 600 UV−vis spectrophotometer (Thermo Scientific, USA) based on the calibration curve obtained in the same solvent. HIP emulsions were produced by vortexing (∼3.2k rpm, 1 min) 1 w/v % aq. SP microfibrils with hexadecane at a 1:9 v/v ratio. The double emulsion was prepared by vortexing (1 min) 1 w/v % SP microfibrils in chloroform with water at a 5:1 v/v ratio, and then vortexing (1 min) with aq. SP colloids at 1 w/v % at a 6:10 v/v ratio.

2.3.1. Light Transmission, Hydrodynamic Diameter, Conductivity, and Surface Tension. The light transmission of 0.01−1% aq. SP or PP colloids and 1% aq. dispersions of ice-templated SPs was measured from 400 to 800 nm using an Evolution 600 UV−vis spectrophotometer (Thermo Scientific, USA), and the first derivative was taken to show the rate of change and wavelength dependence. The hydrodynamic diameters of SP particulates in 0.2−1% colloids were measured with a Zetasizer Nano S90 (Malvern Instruments, UK) at 21 °C to obtain the mean and standard deviation of triplicated measurements. Conductivities of aq. SP colloids at concentrations over four order of magnitudes (0.0005−3.8%) at 21 °C were measured with an OAKTON pH/Con 510 series meter. The critical aggregation concentration (CAC) was determined by the intercept of slopes from two linear regressions of the conductivity versus concentration plots and the average of three reported. Surface tensions of 0.1% aq. dispersions of ice-templated SPs were determined using a platinum plate with 3 mm immersion depth at 21 °C by the Wilhelmy plate method (K100 tensiometer, Kruss GmbH, Germany), and the mean and the standard deviation of five measurements were reported.

2.3.2. Morphologies by SEM, Optical and Atomic Force Microscopy. Ice-templated products from the control and colloids at different concentrations were mounted with the conductive carbon tape and sputter-coated with gold/palladium and observed at 5 kV accelerating voltage using a field emission scanning electron microscope (XL 30-SFEG, FEI/Philips, USA; Quattro, Thermo Scientific, USA). The widths of fibrils in ice-templated products were measured from 50 or 100 individual fibrils to report the means and standard deviations.

The air-dried microfibrils (0.1 w/v %, 10 μL) on glass slides were observed using a Leica DM2500 optical microscope equipped with a cross-polarizing filter to measure their width (N = 150) and length (N = 50), and their means with standard deviations were reported. Supernatants (5k rpm, 15 min) of ice-templated SP dispersions (0.0001 w/v %, 10 μL) in water or EtOH were deposited onto freshly cleaved mica (Highest Grade V1 Mica Discs, Ted Pella, Inc.) and imaged by atomic force microscopy (AFM, MFP-3D, Oxford Instruments Asylum Research, Inc., USA) in the tapping mode with OMCL-AC160TS standard silicon probes (tip radius < 10 nm, spring constant = 28.98 N/m, resonant frequency of ca. 310 kHz) (Olympus Corp., Japan) at 1 Hz scan rate under ambient conditions. The heights of SP nanoparticulates (N = 150) and nanofibrils (N = 50) were analyzed from five to ten 5 μm × 5 μm height images with 512 × 512 pixel resolution using Igor Pro 6.21, and the means and standard deviations were reported.

2.3.3. XRD, FTIR−ATR, Thermal Behavior, and BET. The crystalline structures of ice-templated SPs were determined by X-ray diffraction (XRD) using a Scintag XDS 2000 powder diffractometer with a Ni-filtered Cu Kα radiation (1.5406 Å) at 45 kV anode voltage and 40 mA current. Ice-templated products were compressed between two glass slides into 1 mm thickness, and their diffractograms were recorded from 5 to 40° at a scan rate of 2°/min. Both peak intensity and peak deconvolution analysis were applied to calculate the crystallinity index (CrI) using Peak Fit (Systat Software). The unit cell dimension was calculated based on Bragg's law

$$d_{hkl} = \frac{\lambda}{2 \sin \theta}$$

The crystallite dimension was calculated using the Scherrer equation[13]

$$D_{hkl} = \frac{0.9\lambda}{\mathrm{FWHM} \times \cos \theta}$$

The secondary structure composition of ice-templated SPs and crude SPI was evaluated by Fourier transform infrared attenuated total reflection (FTIR−ATR) analysis on a Nicolet iN10 microscope spectrometer (Thermo Fisher Scientific, USA) using a liquid nitrogen cooled detector. Each spectrum was collected from 1700 to 1600 cm^{-1} at a 4 cm^{-1} resolution. Peaks were deconvoluted with the Levenberg−Marquardt algorithm, and peak areas were calculated using Peak Fit with the Gaussian function (R^2 > 0.99), assuming that each band within the broadened amine I is characteristic of a specific

https://dx.doi.org/10.1021/acsabm.0c00188
ACS Appl. Bio Mater. 2020, 3, 2473−2481

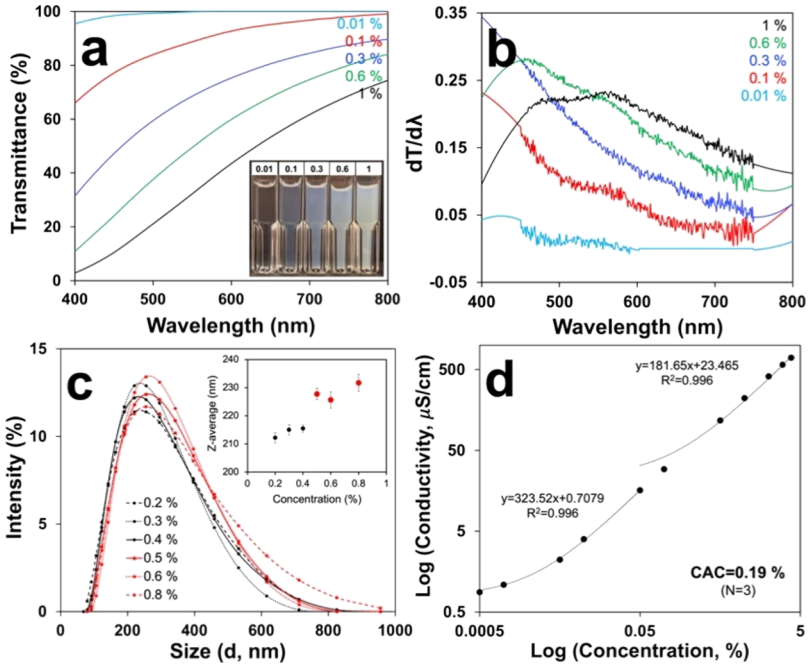

Figure 1. Aq. SP colloids: (a) visible light transmittance, with inserted photographic images; (b) first derivatives of transmittance; (c) hydrodynamic diameter distribution by dynamic light scattering, with the *Z*-average size in the inset; and (d) log–log plot of conductivity over 0.0005 to 3.8% concentration gradient.

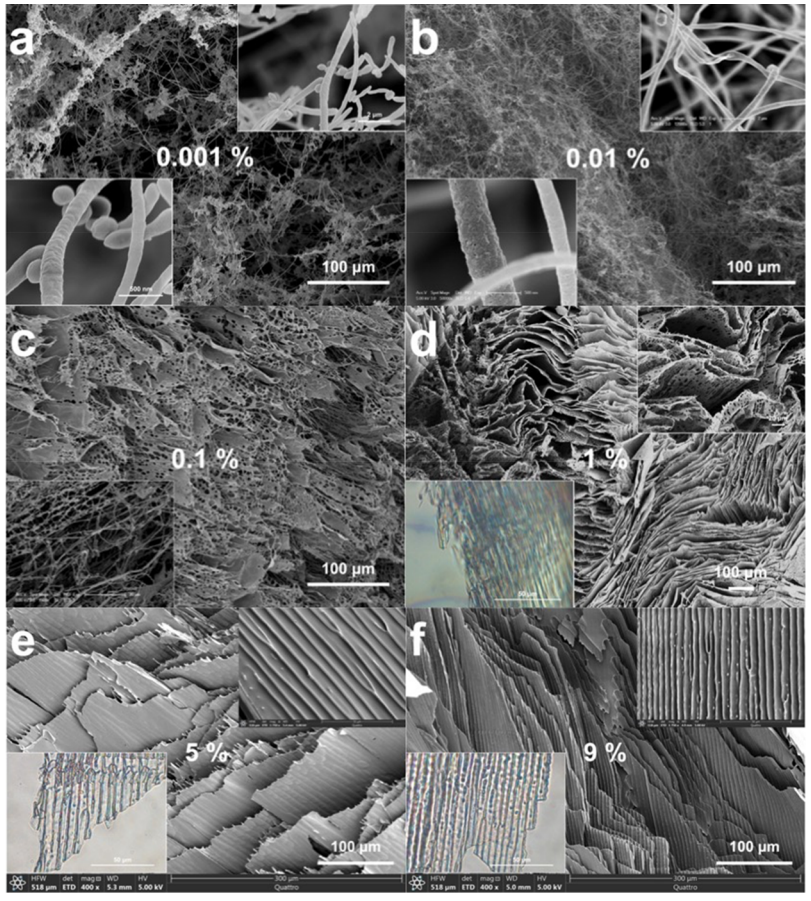

Figure 2. SEM images of longitudinal sections of ice-templated (−196 °C, 5 min, then lyophilized) products of aq. SP colloids at: (a) 0.001, (b) 0.01, (c) 0.1, (d) 1, (e) 5, and (f) 9%. Higher magnification images are inserted in (a–d) and on the upper right in (e,f). The lower left inserts in (d–f) are optical microscopy images.

https://dx.doi.org/10.1021/acsabm.0c00188
ACS Appl. Bio Mater. 2020, 3, 2473−2481

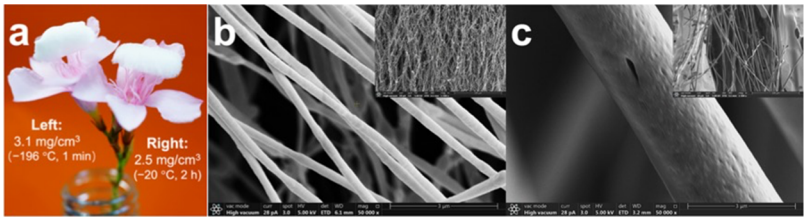

Figure 3. Ice-templated products of 0.1% aq. SP colloids: (a) ultralight fibrous mass on top of an oleander blossom with the densities displayed; SEM images from freezing at (b) −196 °C for 1 min and (c) −20 °C for 2 h.

secondary structure,[14] and the area percentage of a given conformation[15] was reported as the secondary structure composition.

The specific surface area and the pore characteristics of ice-templated products (0.5−1 g) from 0.01, 0.1, 0.6, and 1% aq. SP colloids were determined by N_2 adsorption at 77 K using a surface area and porosity analyzer (ASAP 2000, Micromeritics, USA). The specific surface area was determined by the Brunauer−Emmett−Teller (BET) method from the linear region of isotherms in the 0.06−0.20 relative P/P_0 pressure range. Pore size distributions were derived from the adsorption branch of the isotherms by the BJH method. The total pore volumes were estimated from the amount adsorbed at a relative pressure of P/P_0 = 0.98.

3. RESULTS AND DISCUSSION

3.1. Behavior of Aqueous SP Colloids. Aq. SP colloids were the supernatants (5k rpm, 15 min) facilely produced by high-speed blending (30k rpm, 15 min) of aq. SPI dispersions at up to 9%. These aq. SP colloids remained homogeneous and stable for at least two weeks, in contrast to the aq. SP control (magnetically stirred ∼2k rpm, 1 h) suspensions that readily phase separated. Aq. SP colloids appeared clear at up to 0.01%, transmitting 100% visible light at above 500 nm, became bluish at 0.1% and increasingly opaque at 0.3 and 0.6%, and finally milky at 1%, reducing the transmission at 400 nm more significantly (from 95 to 3%) than that at 800 nm (100 to 74%) (Figure 1a), likely due to Rayleigh scattering. The distinctly lower dependence of light transmission on lower wavelengths shown by the first derivatives of 0.6 and 1% colloids (Figure 1b) coincides with the increasing hydrodynamic sizes of agglomerated SPs from 212−216 nm in 0.2−0.4% to 226−232 nm in 0.5−0.8% aq. colloids (Figure 1c).

Aq. SP colloids also showed a slightly lower linear dependence of electrical conductivity at above 0.19% (Figure 1d), consistent with the reduced charge mobility from increasing sizes of agglomerations. These concentration-dependent behaviors of aq. SP colloids are evidence of self-association and supports the presence of a CAC above which SPs aggregate. This conductivity-derived CAC of 0.19% is equivalent to 0.006 mM, using 280 kDa[3] as the average molecular weight of SPI, which is one-fifth of that (0.98% or 0.035 mM) by surface tension.[5] Such a difference may be attributed to heterogeneous amino acid compositions, highly polydisperse molecular weights (e.g. 8−600 kDa), and varying surface functional groups of SPs. Self-association of amphiphilic SP colloidal nanoparticulates with increasing concentrations is likely entropically driven by the hydrophobic effect to overcome the electrostatic repulsion from surface carboxylates (ζ-potential = −39.1 mV, 0.1%) at above their 4.5 isoelectric point.[16]

3.2. Self-Assembled Structures via Isotropic Freezing and Lyophilization. *3.2.1. Morphology as Affected by SP Concentration and Freezing Rate.* Isotropic freezing and lyophilization of aq. SP colloids produced a white and fluffy mass (Figure S1) in 1D fibrous to ordered 2D laminated structures with increasing concentrations from 0.001 to 9% (Figure 2). Sub-micron wide fibrils (230 ± 88 nm, N = 50) and stringed particulates in almost equal proportions from 0.001% and similarly wide (231 ± 74 nm, N = 100) but longer fibrils from 0.01% were observed (Figure 2a,b). Wider fibrils (618 ± 205 nm, N = 50) among mesh-like structures were observed at 0.1% (Figure 2c); the mesh-like structures increased in proportion from 0.3 to 0.6% (Figure S2); then highly organized laminated layers composed of 1−1.5 μm wide fibers became apparent at 1% (Figure 2d); and finally thicker sheets of similar sized fibers were visible at 2−9% (Figure 2e,f, S2). This orderly fibrillar structural transition from 1D individual fibrils at ≤0.1%, 2D fibrous mesh at 0.1−0.6%, to all laminated fibrous structures at 1−9% appears to be unique to aq. SP colloids upon isotropic freezing. In contrast, upon the same freezing and freeze-drying, the control suspensions produced highly irregular mixtures of micro-particulates, submicron and micron fibers, and ribbons and films, showing no consistent structures or transitions (Figure S3). This orderly fibrillar to laminated fibrillar structural transformation of colloidal SPs from ice-templating is unique and attributed to their significantly small dimensions or larger specific surfaces and amphiphilicity to self-associate inter-facially with increasing concentrations. It should be noted that while others had reported isotropic freezing and freeze-drying of SP gels into porous substrates[16,17] and directional freezing and lyophilization of guanidine hydrochloride (6 M) denatured SPI into 2−4 μm wide microfibrils (1%), non-fibrous lamellas (4−7%), and cellular (>10%) structures,[18] none observed similar orderly transitions. The intriguing nature of these intrafibril and interfibril interfaces is thus further analyzed next.

The effect of ice-templating was further observed by accelerating freezing in ca. 1000 times more thermally conductive aluminum tubes or slowing the freezing at a higher freezing temperature (Figure 3a−c). Liquid nitrogen freezing of 0.1 and 1% aq. SP colloids in aluminum was faster (1 min) and lyophilized into finer 258 nm (±48 nm, N = 100) wide fibrils and laminated fibrous structures containing 600−900 nm wide fibrils (Figure S4), respectively, approximately half in width as those from the less thermally conductive polypropylene tubes (618 nm and 1−1.5 μm, Figure 2). Freezing at −20 °C took longer (2 h) and produced one magnitude wider (2279 ± 271 nm, N = 100) fibrils at 0.1% and an ultralight fibrous mass with a merely 2.5 mg/cm^3 density. Rapid freezing nucleates ice quickly and forms numerous, much smaller ice crystals to segregate SPs in many narrow spaces, whereas slow freezing allows ice nuclei to grow into larger crystals, concentrating SPs to assemble into a fewer, but larger mass. Therefore, the widths of fibrils assembled can be easily controlled by freezing rates, whereas the extent of 1D fibrous

https://dx.doi.org/10.1021/acsabm.0c00188
ACS Appl. Bio Mater. 2020, 3, 2473−2481

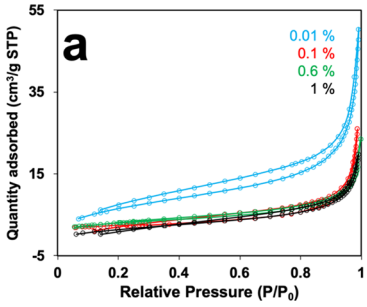

b Sample	BET surface area (m^2/g)	Total pore volume ($\times 10^{-3}$ cm^3/g)	t-Plot external surface area (m^2/g)
0.01 %	26.7	5.98	37.5
0.1 %	8.23	2.76	6.51
0.6 %	11.4	2.49	13.7
1 %	13.5	2.57	16.2

Figure 4. N_2 adsorption and desorption of ice-templated (−196 °C, 5 min) products from 0.01, 0.1, 0.6, and 1% aq. SP colloids: (a) isotherms at 77 K and (b) BET surface areas and pore characteristics.

to 2D laminated structures can be varied by aq. SP colloid concentrations.

3.2.2. Specific Surface, Pores, and Crystalline Structures. The ice-templated products from 0.01 to 1% SP colloids exhibited type II adsorption isotherms, typical of nonporous or macroporous structures (Figure 4a). The same type H3 hysteresis loop without a plateau at high P/P_0, usually corresponding to slit-shaped pores,[19] was observed irrespective of varying fibril widths and mesh-to-laminate structures, suggesting the fibrillar structure to be the dominant nonporous domains in the progressively assembled structures with increasing SP concentrations. The finest fibrils (231 nm) assembled at 0.01% had the highest BET specific surface area of 26.7 m^2/g, two to three times that of higher concentrations (Figure 4b). Both specific surface area and pore volume reduced with increasing concentrations from 0.01 to 0.1%, consistent with their, respectively, enlarging fibril widths from 230.9 to 618 nm, further widening to 1−1.5 μm fiber width (1%), then to more compact 2D structures above 1%. The ice-templated products showed a lower crystalline index (CrI = 45 or 47%) than both the control (CrI = 60 or 58%) and crude SPI (CrI = 71 or 70%) (Figures S5 and S6, Table S1), as expected from reduced colloidal particulate sizes from the shear force and heat in high-speed blending. The lower crystallinity is also consistent with 20% less β-domains based on the analyses of FTIR amide I bonds (Figure S5).

3.3. Dispersion of Self-Assembled SPs in Water and Organic Solvents. The ice-templated laminated fibrous product from 1% aq. SP colloids was dispersed in organic solvents with different polarities and H-bonding abilities to probe the nature of self-assembled interfaces. Ice-templated SPs were fully dispersed in water, by hand shaking alone, into a uniform and translucent aq. dispersion with ca. 15 v/v % foams (Figure 5a). Brief sonication (130 W, 5 min) could also homogeneously disperse ice-templated SPs in DMF, MeOH, EtOH, and acetone with increasing opaqueness, suggesting an increase in disassembled sizes, but disperse only partially in chloroform or toluene and none in hexane (Figure 5b). After 1 h, the aq. dispersion showed trace amounts of precipitates, whereas organic dispersions showed varying levels of phase separation (Figure 5c). After 1 d, only the aq. dispersion remained the same, while others nearly fully settled (Figure 5d). In contrast, crude SPI could not be dispersed in any of these liquids even with sonication and completely settled within 1 h (Figure S6). The fact that ice-templated SPs are fully water-dispersible with simple hand shaking and remarkably dispersible in polar organic solvents by sonication indicates polar interactions to be dominant at the assembled interfaces.

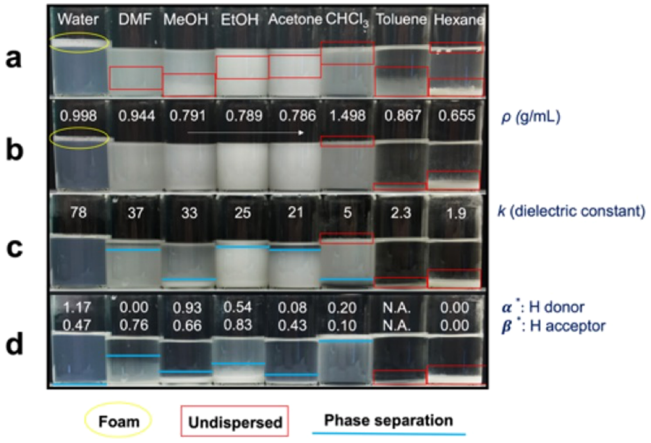

Figure 5. Dispersibility of ice-templated (−196 °C, 5 min) products from 1% aq. SP colloids in water and organic liquids with parameters displayed at 0.1 w/v % from: (a) hand-shaking for seconds; (b) sonication (130 W, 5 min); (c,d) (b) settled for 1 h (c) or 1 d (d). *α, a measure of the H-bond donor from the UV/vis spectrum of 4-nitroaniline that was sensitive to hydrogen bond donation from the $-NH_2$ group.[20] *β, a measure of the H-bond acceptor from dye studies in protic solvents by subtracting the polarity and the polarizability effect.[20]

The aqueously re-dispersed ice-templated SPs were slightly more hydrophobic and less surface active, exhibiting a larger concave meniscus inside of hydrophobic polystyrene cuvette surfaces and a slightly lower surface tension (48.1 ± 0.6 mN/m, N = 5) at 0.1% than the original colloid (50.6 ± 0.5 mN/m, N = 5). Their lower transparency and absence of Tyndall phenomenon as the original aq. colloids at 1% (Figure S7) also suggest less uniform particulate sizes. In fact, nearly three-quarters (73.7%) of the re-dispersed ice-templated SPs were in the supernatant and appeared as 4.3 nm (±4.8 nm, N = 100) thick nanoparticulates (Figure S8), similar to those in original colloids (6.0 ± 8.0 nm), whereas the precipitates (26.3%) contained much larger microfibrils and mesh-like structures (Figure S9). While self-association of amphiphilic SP nanoparticulates in water is thought to be driven by hydrophobic interactions as discussed earlier, hydrophobic interactions contribute less or only partially in the nanoparticular interfaces, as evident by only a quarter of ice-templated SPs being indispersible in water. The ice-templated SP remained as mesh-like fibrous pieces in chloroform and toluene even after extended sonication (15 min) (Figure S10) and not dispersible in hexane, further affirming insignificant non-polar interaction from ice-templating.

https://dx.doi.org/10.1021/acsabm.0c00188
ACS Appl. Bio Mater. 2020, 3, 2473−2481

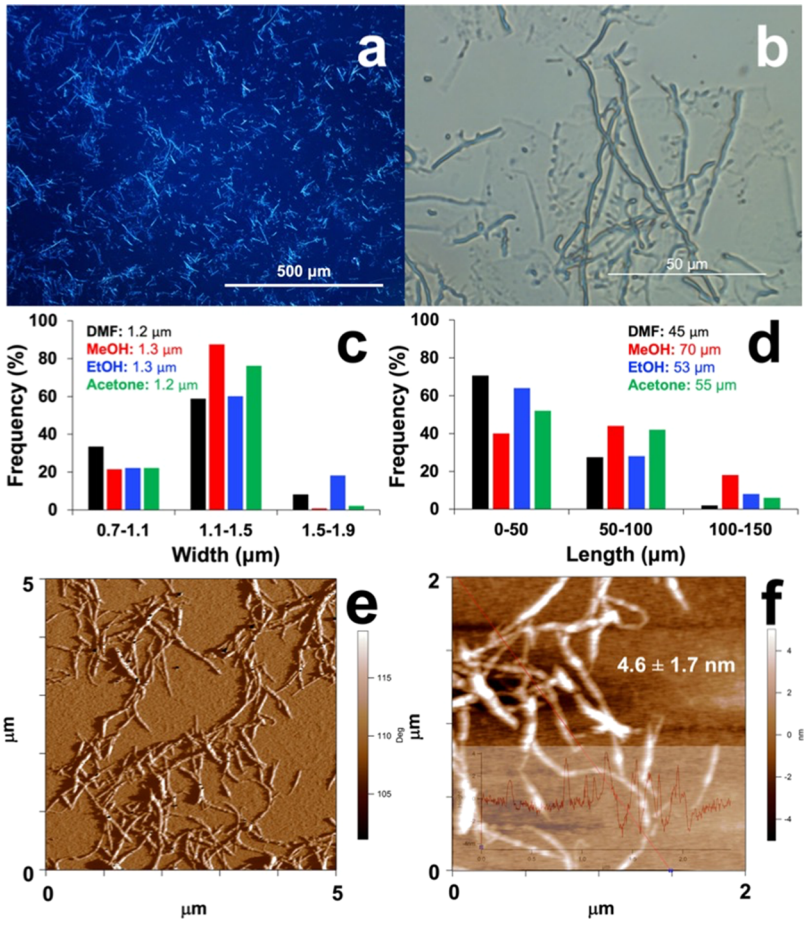

Figure 6. Microfibrils in the supernatant (5k rpm, 15 min) of EtOH dispersions of ice-templated (−196 °C, 5 min) products of 1% aq. SP colloids: (a) optical microscopy image under crossed polar light; (b) optical microscopy image; (c) width (N = 150); (d) length (N = 50); (e) AFM phase image; and (f) AFM height image with the height profile.

Impressively, polar solvents like DMF, MeOH, EtOH, and acetone much effectively dispersed the laminated fibrous structures of ice-templated SPs into mostly microfibrils with a few micro-particulates and film-like pieces (Figure S11). With lower dielectric constants and weaker H-bonding ability, especially as H donors (Figure 5), these polar organic solvents are far less polar than water and cannot interrupt H-bonding like water to disintegrate microfibrils into particulates. These observations suggest that strong H-bonding dominates at the interfaces among colloidal nanoparticulates within the fibrils, whereas the weaker forces (i.e. van der Waals, dipole−dipole, etc.) may be more prevalent at the inter-fibril interfaces. Microfibrils in EtOH not only revealed strong birefringence under crossed polar light, but also exhibited flow birefringence when gently shaken or stirred to create a shear flow (Figure 6a and S12). Overall, 1.2−1.3 μm wide and 45−70 μm long microfibrils (Figure 6c,d, Table S2) were produced from dispersing the ice-templated laminates in all polar solvents employed here. The widths of these microfibrils were consistent with those (1−1.5 μm) observed in ice-templated SPs (Figure 2d), and may be tunable by simply adjusting the freezing conditions, as demonstrated earlier.

The ice-templated SPs dispersed in EtOH were then precipitated by centrifugation into nearly all (98.5%) microfibrils with 1.3 μm (±0.3 μm, N = 150) width and 53 μm (±30 μm, N = 50) length (Figure 6a−d). The merely 1.5% in the supernatant appearing as nanofibrils with 4.6 nm (±1.7 nm, N = 50) height (Figure 6e,f) and less than 3 nm thick nanoparticulates (Figure S13) may be attributed to the lower molecular mass SP fractions. While the microfibrils in EtOH fully settled in hours, they could be redispersed uniformly by hand shaking and retained their fibrous morphology when stored at ambient temperature for months, affirming their highly stable structure. The SP microfibrils precipitated from EtOH could also be homogeneously redispersed in water, non-polar chloroform or toluene (Figure S14), and an EtOH/hexane (2:1, v/v) mixture (not shown), but not in hexane. This versatile dispersibility of SP microfibrils in protic (water, MeOH, and EtOH), aprotic (DMF and acetone), polar, and non-polar (chloroform and toluene) solvents gives clear evidence of their amphiphilic characteristics.

3.4. Amphiphilicity of Microfibrils: Dye Binding and Pickering Emulsion. The unique amphiphilic characteristics of SP microfibrils were further demonstrated as carriers for hydrophobic SR and CR lipophiles and cationic MB electrophiles. First, all three lipophiles and electrophiles could be homogeneously dispersed in water at 0.8 mM with the aid of amphiphilic aq. SP colloids. Upon freezing and freeze-drying, the dye-bound ice-templated products could also be dispersed in water into microfibrils in similar dimensions as those without the dyes (Figure 7a−c), showing no interference of the bound dyes on the self-assembly of SP colloidal particulates or the subsequent dispersion in EtOH. Based on the quantities of dyes dissolved in EtOH or acetone, nearly

https://dx.doi.org/10.1021/acsabm.0c00188
ACS Appl. Bio Mater. 2020, 3, 2473−2481

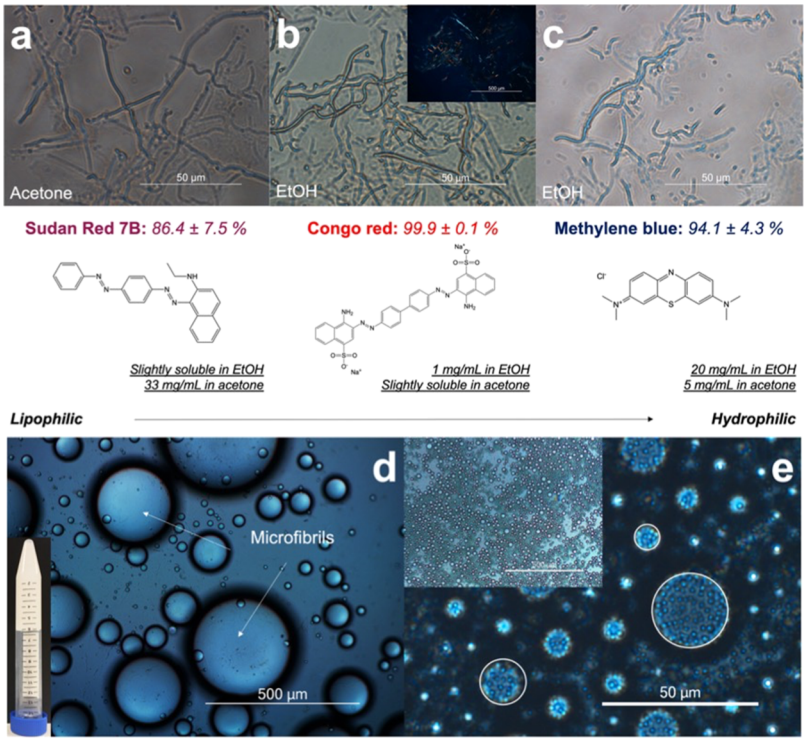

Figure 7. Amphiphilic behaviors of dye-bound SP microfibrils (0.8 mM dye, 0.04 mM SPs): optical images of (a) SR-, (b) CR-, (c) MB-bound SP microfibrils dispersed in acetone or EtOH with dye solubility displayed and under a cross-polar micrograph inserted in (b); (d) HIP o/w Pickering emulsion gel (ϕ = 90%, hexadecane) with 1 w/v % aq. SP microfibrils (inset: photograph of gel after 3 d); (d) double $w_1/o/w_2$ Pickering emulsion (o: 1 w/v % SP microfibrils in chloroform; w_2: 1 w/v % aq. SP colloids).

100% CR, 94.1% MB, and 86.4% SR were retained with SP microfibrils. The highest binding efficiency of CR may be attributed to its ability to bind SPs via both hydrophilic and hydrophobic interactions. While SP microfibrils were bluish under crossed polar light (Figure 6a), CR bound SP microfibrils appeared in varying apple-green, yellowish, or reddish birefringence, depending on the orientation of microfibrils (Figure 7b), showing altered light refraction from the bound CR. Most importantly, these lipophilic and electrophilic dye-bound SP microfibrils remain amphiphilic, showing essentially unchanged dispersibility in polar and nonpolar solvents. Such robust amphiphilic characteristics demonstrate these SP microfibrils to be excellent carriers for other lipophiles and electrophiles.

Amphiphilic SP microfibrils can also function as robust Pickering emulsifiers, capable of emulsifying 90/10 v/v hexadecane/water or HIP o/w emulsion by simply vortexing (Figure 7d). This gel-like HIP emulsion remained stable at ambient temperatures for at least 3 d, clearly showing the superior amphiphilicity of SP microfibrils adsorbed at the o/w interfaces and wrapped around the droplets without even full coverage. Furthermore, $water_1/oil/water_2$ ($w_1/o/w_2$, 1:5:10 v/v/v) double Pickering emulsions were also possible with 1 w/v % SP microfibrils in the oil phase (chloroform) and 1 w/v % aq. SP colloid as w_2, forming type C droplets encapsulating numerous smaller internal aq. phase droplets (Figure 7e). To date, only glutaraldehyde crosslinked gelatin particles (ca. 200 nm wide, 0.5−1.5%)[21] and anti-solvent precipitated gliadin particles (3855 nm wide, 2%)[22] have been reported as protein-based HIP Pickering emulsifiers that stabilized merely 80 v/v % hexane[22] and corn oil.[23] To the best of our knowledge, these SP microfibrils are the first report of protein fibrillar amphiphiles as Pickering emulsifiers for facilely stabilizing HIP as well as double emulsions.

3.5. Colloids by Sonication and Applicability to Pea Proteins. Briefly, 5 min of probe sonication (60 W, ca. 17 kJ) also dispersed over 90% SPI into aq. colloids at up to 9%. The sonicated colloids appeared less transparent than those obtained from high-speed blending at the same concentration, but became similarly translucent by doubling the power (Figure S15a). These sonicated colloids, including those that were not dialyzed, could also generate microfibrils at a nearly full yield from the same isotropic freezing, freeze-drying, and EtOH-dispersing process (Figure S15b,c). The fact that salts used during protein extraction and isolation shows no interference to microfiber production further simplifies the process.

Sonication was also applied to produce aq. colloids from yellow pea proteins (PPs, ca. 200 k*Da*), another globular legume protein that contains similar polar AAs (59%) as SPs (60%), but higher 7S (ca. 48%) and lower 11S (ca. 37%) than SPs.[23] The sonicated (60 W, 5 min) 1% aq. PP colloids transmitted far less light (Figure S16) than either sonicated (Figure S15a) or blended SPs (Figure 1a), for example, 6% versus 60 and 74% at 800 nm, respectively, indicative of larger colloidal particulate sizes. These PP colloidal particulates also tend to self-associate at a lower 0.1% concentration, as evident from the first derivative of light transmittance (Figure S16). The ice-templated structures from PP colloids were also concentration-dependent, that is, ultra-fine 381 nm (±67 nm, N = 50) wide fibrils from 0.1%, both 1D fibrils and 2D mesh-like fibrous structures from 0.3 to 1%, and all laminated fibrous mass from 2% (Figure S17). Dispersing the ice-templated product from 2% PP colloids in EtOH also generated

https://dx.doi.org/10.1021/acsabm.0c00188
ACS Appl. Bio Mater. 2020, 3, 2473−2481

microfibrils (Figure S18) that were 1.1 μm ($\pm$0.2 μm, N = 150) wide or ca. 20% thinner than those from SPs (Figure 6a,c). These PP microfibrils can also be redispersed in water, chloroform, and toluene (not shown). Therefore, mechanical shear by sonication, ice templating, and EtOH dispersion approach were also applicable to produce amphiphilic protein microfibrils from other similar globular legume proteins.

4. CONCLUSIONS

Aqueous SP colloids, facilely processed by either high-speed blending or sonication, have shown to be amphiphilic, and can self-associate into micelle-like structures in water at above 0.19, 0.4, and 0.98%, as determined by conductivity, dynamic light scattering, and surface tension, respectively. Ice-templated self-assembling of amphiphilic SP colloids produced concentration-dependent 1D to 2D fibrous structures, from ca. 230 nm wide fibrils at up to 0.01% to sub-micron wide fibrils in mesh-like structures to 1−1.5 μm wide fibers in laminated structures at 1−9%. Nearly three-quarters of the self-assembled SPs could be reverted back to colloidal nanoparticulates in water, affirming the dominant role of H-bonding at inter-nanoparticulate interfaces. Most intriguingly, these self-assembled SPs could be fully dispersed in polar protic (e.g., alcohols) and polar aprotic (e.g., DMF, acetone) solvents into ca. 1.2 μm wide semicrystalline microfibrils. These SP microfibrils are amphiphilic, i.e., homogeneously dispersible in water and in nonpolar chloroform and toluene as well as binding lipophilic and electrolytic dyes equally and efficiently. This mechanical shear or sonication, ice templating, and EtOH dispersion approach of producing amphiphilic microfibrils was also validated with another globular legume pea protein. Most significantly, these protein microfibrils have demonstrated to be robust amphiphiles for HIP and double emulsions as well as potential carriers for lipophiles and electrophiles. This ice-templated self-assembling and polar solvent disassembling approach offers a facile and scalable way to convert the abundant and under-utilized globular protein byproducts of oil and biofuel into uniquely amphiphilic protein microfibrils as high-performance Pickering emulsifiers for many potential consumer and industrial applications. As SP is natural and the process is green, these microfibrillar amphiphiles are excellent emulsifiers, particularly they are desirable for human ingestion such as in foods, pharmaceuticals and skin care.

■ ASSOCIATED CONTENT

Supporting Information

The Supporting Information is available free of charge at https://pubs.acs.org/doi/10.1021/acsabm.0c00188.

SEM images, FTIR−ATR, XRD, and DTG of ice-templated SPs; AFM and optical images of disassembled ice-templated SPs; colloidal characterization of PPs; and SEM images of ice-templated PPs (PDF)

■ AUTHOR INFORMATION

Corresponding Author

You-Lo Hsieh − *Biological and Agricultural Engineering, University of California, Davis, California 95616, United States;* orcid.org/0000-0003-4795-260X; Email: ylhsieh@ucdavis.edu

Author

Xingchen Liu − *Biological and Agricultural Engineering, University of California, Davis, California 95616, United States;* orcid.org/0000-0002-1011-5771

Complete contact information is available at: https://pubs.acs.org/10.1021/acsabm.0c00188

Notes

The authors declare no competing financial interest.

■ ACKNOWLEDGMENTS

The authors appreciate the funding support from Henry A. Jastro Research Award, University of California, Davis and USDA National Institute of Food and Agriculture, Hatch project CA-D-6706.

■ REFERENCES

(1) Service, F. A. *Oil Seeds: World Market and Trade*; U.S. Department of Agriculture, 2018.

(2) Barrett, J. R. The science of soy: what do we really know? *Environ. Health Perspect.* **2006**, *114*, A352.

(3) Nishinari, K.; Fang, Y.; Guo, S.; Phillips, G. O. Soy proteins: A review on composition, aggregation and emulsification. *Food Hydrocolloids* **2014**, *39*, 301−318.

(4) Reddy, N.; Yang, Y. Potential of plant proteins for medical applications. *Trends Biotechnol.* **2011**, *29*, 490−498.

(5) Liu, X.; Hsieh, Y.-L. Amphiphilic and amphoteric aqueous soy protein colloids and their cohesion and adhesion to cellulose. *Ind. Crops Prod.* **2020**, *144*, 112041.

(6) Wang, Y.; Xu, H.; Zhang, X. Tuning the Amphiphilicity of Building Blocks: Controlled Self-Assembly and Disassembly for Functional Supramolecular Materials. *Adv. Mater.* **2009**, *21*, 2849−2864.

(7) Israelachvili, J. N.; Mitchell, D. J.; Ninham, B. W. Theory of self-assembly of lipid bilayers and vesicles. *Biochim. Biophys. Acta Biomembranes* **1977**, *470*, 185−201.

(8) Mezzenga, R.; Fischer, P. The self-assembly, aggregation and phase transitions of food protein systems in one, two and three dimensions. *Rep. Prog. Phys.* **2013**, *76*, 046601.

(9) Chen, N.; Zhao, M.; Chassenieux, C.; Nicolai, T. Structure of self-assembled native soy globulin in aqueous solution as a function of the concentration and the pH. *Food Hydrocolloids* **2016**, *56*, 417−424.

(10) Tang, C.-H.; Wang, C.-S. Formation and Characterization of Amyloid-like Fibrils from Soy β-Conglycinin and Glycinin. *J. Agric. Food Chem.* **2010**, *58*, 11058−11066.

(11) Jiang, F.; Han, S.; Hsieh, Y.-L. Controlled defibrillation of rice straw cellulose and self-assembly of cellulose nanofibrils into highly crystalline fibrous materials. *RSC Adv.* **2013**, *3*, 12366−12375.

(12) Jiang, F.; Hsieh, Y.-L. Assembling and redispersibility of rice straw nanocellulose: effect of tert-butanol. *ACS Appl. Mater. Interfaces* **2014**, *6*, 20075−20084.

(13) Scherrer, P. Estimation of the size and internal structure of colloidal particles by means of röntgen. *Nachr. Ges. Wiss. Göttingen* **1918**, *2*, 96−100.

(14) Byler, D. M.; Susi, H. Examination of the secondary structure of proteins by deconvolved FTIR spectra. *Biopolym.: Orig. Res. Biomol.* **1986**, *25*, 469−487.

(15) Goormaghtigh, E.; Cabiaux, V.; Ruysschaert, J.-M. Secondary structure and dosage of soluble and membrane proteins by attenuated total reflection Fourier-transform infrared spectroscopy on hydrated films. *Eur. J. Biochem.* **1990**, *193*, 409−420.

(16) Arboleda, J. C.; Hughes, M.; Lucia, L. A.; Laine, J.; Ekman, K.; Rojas, O. J. Soy protein-nanocellulose composite aerogels. *Cellulose* **2013**, *20*, 2417−2426.

(17) Zhuang, Y.; Yu, F.; Ma, J.; Chen, J. Facile synthesis of three-dimensional graphene−soy protein aerogel composites for tetracycline adsorption. *Desal. Water Treat.* **2016**, *57*, 9510−9519.

(18) Guan, J.; Porter, D.; Tian, K.; Shao, Z.; Chen, X. Morphology and mechanical properties of soy protein scaffolds made by directional freezing. *J. Appl. Polymer Sci.* **2010**, *118*, 1658−1665.
(19) Thommes, M.; Kaneko, K.; Neimark, A. V.; Olivier, J. P.; Rodriguez-Reinoso, F.; Rouquerol, J.; Sing, K. S. W. Physisorption of gases, with special reference to the evaluation of surface area and pore size distribution (IUPAC Technical Report). *Pure Appl. Chem.* **2015**, *87*, 1051−1069.
(20) Anslyn, E. V.; Dougherty, D. A. *Modern Physical Organic Chemistry*; University Science: Sausalito, CA, 2006.
(21) Tan, H.; Sun, G.; Lin, W.; Mu, C.; Ngai, T. Gelatin particle-stabilized high internal phase emulsions as nutraceutical containers. *ACS Appl. Mater. Interfaces* **2014**, *6*, 13977−13984.
(22) Hu, Y.-Q.; Yin, S.-W.; Zhu, J.-H.; Qi, J.-R.; Guo, J.; Wu, L.-Y.; Tang, C.-H.; Yang, X.-Q. Fabrication and characterization of novel Pickering emulsions and Pickering high internal emulsions stabilized by gliadin colloidal particles. *Food Hydrocolloids* **2016**, *61*, 300−310.
(23) Barac, M.; Cabrilo, S.; Pesic, M.; Stanojevic, S.; Zilic, S.; Macej, O.; Ristic, N. Profile and functional properties of seed proteins from six pea (Pisum sativum) genotypes. *Int. J. Mol. Sci.* **2010**, *11*, 4973−4990.

https://dx.doi.org/10.1021/acsabm.0c00188
ACS Appl. Bio Mater. 2020, 3, 2473−2481